Korean J. Chem. Eng., 36(7), 1069-1081 (2019)
DOI: 10.1007/s11814-019-0285-z

pISSN: 0256-1115
eISSN: 1975-7220

A comparative study on dynamic Hg(II) and MeHg(II) removal by functionalized agrowaste adsorbent: breakthrough analysis and adsorber design

Norasikin Saman*, Helen Kong, Safia Syazana Mohtar*, Khairiraihanna Johari***, Azmi Fadziyana Mansor*, Onn Hassan*, Noorhalieza Ali*, and Hanapi Mat*,****,†**

*Advanced Materials and Process Engineering Laboratory, School of Chemical and Energy Engineering, Faculty of Engineering, Universiti Teknologi Malaysia, 81310 UTM Skudai, Johor, Malaysia
**Centre of Lipid Engineering and Applied Research, Level 2, Block C08, Faculty of Science, Universiti Teknologi Malaysia, 81310 UTM Skudai, Johor, Malaysia
***Department of Chemical Engineering, Faculty of Engineering, Universiti Teknologi PETRONAS, 32610, Bandar Seri Iskandar, Perak, Malaysia
****Advanced Materials and Separation Technologies (AMSET) Research Group, Health and Wellness Research Alliance, Universiti Teknologi Malaysia, 81310 UTM Skudai, Johor, Malaysia
(*Received 7 November 2018 • Accepted 27 April 2019*)

Abstract−The adsorption dynamics of inorganic mercury, Hg(II) and organic methylmercury, MeHg(II) removal by low-cost reactive agrowaste adsorbents namely CP-Pure, CP-MPTES and CP-RR was investigated in a fixed-bed adsorber. The results show that the breakthrough and saturation times were delayed with decreasing flow rate (F) and initial concentration (C_o), and increasing bed height (Z). The Hg(II) possessed better adsorption performance than MeHg(II). The isotherm and kinetic model analyses of adsorption data followed the Temkin isotherm and the pseudo-second order kinetic models, respectively. The breakthrough curve was simulated well by the Thomas and Yoon-Nelson models, and then was further used for scale-up studies. The empty bed contact time (EBCT) concept was successfully demonstrated for the adsorber design and scale-up studies. The regeneration studies showed that the regenerated CP-Pure and CP-MPTES have a high regeneration efficiency up to third adsorption cycle.

Keywords: Agrowaste, Fixed-bed, Inorganic Mercury, Organic Mercury, Breakthrough Curve

INTRODUCTION

The release of mercury in liquid phase is considered small relative to the vapor phase; however, it can significantly affect the environment [1]. Inorganic (e.g., HgCl) and organic (e.g., methylmercury and dimethyl mercury) forms of mercury are normally present in the liquid phase. The inorganic mercury is less toxic than organic mercury, but it is easy to transform into more toxic methylmercury in the presence of bio-compound activity in water/wastewater. Due to the severe effect of mercury on human health, the removal of mercury in effluent discharged is important, and adsorption is found to be the most appealing process. In the past ten years, several studies have been conducted to develop an effective adsorbent using agricultural wastes [2-9], marine resources [10], living biomass [11], carbons/chars [6,12-14], polymers [15,16], and oxide materials [17-20] to remove mercury ions from aqueous solutions.

So far, the research activities in the field of mercury removal are primarily focusing on the adsorbent development, and the effectiveness of adsorbent was defined by its maximum adsorption capacity, adsorption rate and selectivity, carried out in a batch adsorption system. The batch system, however, is considered uneconomical for practical applications, because it requires a large amount of adsorbent for a large volume of effluent [21]. The adsorption performance is also highly influenced by the initial concentration rather than the effluent concentration [22]. In a batch system, the solute remains in contact until equilibrium is achieved between solute in solution and solute in a given quantity of adsorbent. In a continuous system, the solute continuously enters and leaves the adsorber; therefore, complete equilibrium between solutes in the solution and in the adsorbent is never achieved. The continuous adsorption performance is judged by the effluent concentration and break point (where the effluent concentration start rising with time), often portrayed as a breakthrough curve analysis.

Continuous adsorption data and accurate forecast of breakthrough curve from a lab-scale system are important for designing the adsorption column. Two modeling approaches, the bed depth service time (BDST) and the empty bed contact time (EBCT), were widely used to predict the breakthrough curves of the scale-up adsorber. The BDST model was initially developed from the modified Bohart-Adam model [23]. The model is suitable if the breakthrough curve obeys the Bohart-Adam model. The model suggests a linear dependency of bed height (Z) with service time. This model has been used by many researchers to determine the service time of the scale-up adsorber [24-27]. On the other hand, the EBCT explains the linear relationship between the Z and velocity (v) of feed solution, which is another vital parameter needed to design an adsorber. The

†To whom correspondence should be addressed.
E-mail: hbmat@cheme.utm.my

change of bed height, bed diameter and flow rate of the scale-up adsorber will affect the EBCT values [28-30]. The literature reporting on using the EBCT technique to simulate the service time of the scaling up adsorber is very limited. Studies conducted by Trgo et al. [30] show the EBCT values have good simulation curves for a scaling up of the laboratory experiment of lead removal by natural zeolites. Song et al. [7] also observed a good simulation curve of the scale up adsorber in a wide range of EBCT values.

This study is a continuation of our previous research on a batch Hg(II) and MeHg(II) adsorption using coconut pith modified with mercaptopropyltriethoxysilane and Reactive Red 120 [4,8]. The adsorbents CP-MPTES and CP-RR, respectively, showed an excellent adsorption performance towards both inorganic and organic mercury species compared to other low-cost adsorbents. The comparative adsorption behavior of both organic and inorganic mercury ions in a continuous adsorption was hardly reported, and the majority of the studies mainly focused only one mercury species in a batch adsorption system. In this study, variations of column operating parameters like bed height (Z), feed solution flow rate (F) and initial mercury ion concentration (C_o) were conducted to further demonstrate the prospects of those adsorbents for industrial applications as well as understanding the fundamental aspects of Hg(II) and MeHg(II) adsorption in the continuous packed-bed adsorber. Adsorbent regeneration studies were also conducted to demonstrate its reusability.

MATERIALS AND METHODS

1. Adsorbents Preparation and Characterization

Agrowaste of coconut pith (CP) was obtained from a local company (T&H Coconut Fiber Sdn. Bhd., Johor, Malaysia). The CP was sieved into particle size range of between 75 μm and 100 μm prior to any treatments. The CP was washed repeatedly using double-distilled (DI) water and dried in an oven at 50 °C and further dried in a vacuum oven. This sample is denoted as CP-Pure. The CP-Pure was further modified using 3-mercaptopropyltriethoxysilane (MPTES) and Reactive Red 120 (RR) to improve its adsorption performance towards mercury species. The CP-MPTES was prepared according to the procedure reported previously [4]. About 0.5 g of CP-Pure was immersed in a pre-hydrolyzed MPTES solution and stirred for 2 h at room temperature. The mixture was then heated at 80 °C for curing process. The CP-MPTES adsorbent was washed thoroughly with DI water and oven dried. The modification of CP-Pure using RR was carried out by mixing 2 g of CP-Pure into a 70 mL of NaCl/RR solution. After an hour of mixing, 30 mL of Na_2CO_3 solution was added into the mixture and the flask was heated to 80 °C and mixed for another 7 h. Then, the CP-RR product was washed and vacuum dried. The detailed procedure was reported in our previous publication [8].

The morphology of the adsorbents was analyzed using a scanning electron microscope (JEOL model JSM-6390LV). The surface area was determined by nitrogen adsorption desorption measurement analyzed using a surface analyzer (Micromeritics ASAP 2002). The functional groups present in the adsorbents were analyzed by a Fourier transform infrared (FTIR) spectrometer (PerkinElmer Model 2000), determined using a KBr disk method. The solid addition method was used to determine the pH at point zero charge (pH_{pzc}) according to the solid addition method. The detailed procedures can be found in our previous publications [4,8,9].

2. Adsorption Procedure

2-1. Preparation of Adsorbate

The stock Hg(II) solution was prepared by dissolving the required amount of $Hg(NO_3)_2{\cdot}H_2O$ (99%) salt in acidified deionized (DI) water. The MeHg(II) solution was prepared by dissolving CH_3HgCl (13% Cl) salt in 1% (v/v) methanol in DI water. The stock solution was then diluted to a desired concentration using DI water. All chemicals used were of analytical reagent grade.

2-2. Adsorption Dynamics Experiment

An adsorption dynamics experiment was carried out using a glass column of 1.0 cm internal diameter. The column was fitted with an adjustable flow adapter to hold the column to a desired adsorbent bed height. The feed solution was flowed downward at a specified flow rate controlled by using a Masterflex Cole Palmer peristaltic pump (USA) that was connected with a silicone tubing size of 16. The effluent was collected at selected time intervals and the mercury ion concentration was determined by using a PerkinElmer Precisely HGA 900 atomic absorption spectrophotometer (AAS, USA). The solution was allowed to flow into the adsorber until the mercury ion concentration in the effluent exceeded 95% of the initial mercury ion concentration in which, at this condition, the adsorber is considered to be saturated.

The adsorption data were evaluated based on the breakthrough curves, which are expressed as a normalized concentration of effluent at time, t=t (C_t) to inlet concentration at t=0 (C_o) as a function of time (i.e. C_t/C_o versus t) or effluent volume (i.e. C_t/C_o versus V_{eff}) [6]. The time required to attain a breakpoint at which the C_t is equal to 10% of C_o (or C_t/C_o=0.1) is referred to as a breakthrough time (t_b). While, the saturation or exhaustion time (t_s) is defined as the time at which the effluent reaches 95% of C_o (or C_t/C_o=0.95).

The total quantity of the adsorbed mercury, q_{total} (mmol) was calculated by using Eq. (1). The integration term in Eq. (1) is basically given by the area above the curves of C_t/C_o versus t up to t_s. The adsorption capacity of mercury ions up to t_s is also known as a saturated adsorption capacity, Q_s (mmol g^{-1}), and can be calculated according to the Eq. (2).

$$q_{total} = FC_o \int_{t=0}^{t=t_s} (1 - C_t/C_o)dt \quad (1)$$

$$Q_s = q_{total}/m \quad (2)$$

where F is the feed solution flow rate (L min^{-1}), C_o and C_t are the concentrations of mercury ion (mM) at time t=0 (min) and t=t (min), respectively.

2-3. Adsorbent Reusability Experiment

After the first cycle of the adsorption process, the saturated adsorbent bed was regenerated (or eluted) using two regeneration solutions: potassium iodide (KI, 0.1 M) and hydrochloric acid (HCl, 0.1 M). The regeneration solution flow rate was 5 mL min^{-1}. The flow of the regeneration solution ceased when the mercury ion concentration in the effluent reached a constant value. The DI water was then passed through the adsorber to flush out the remaining regeneration solution in the adsorbent bed before the subsequent

adsorption experiment.

The adsorbent reusability was evaluated by carrying out an adsorption-desorption experiment. The experiment was carried out up to five cycles of adsorption. In each cycle, the adsorption and desorption experiments were carried out using the same conditions and regeneration solution. The adsorption performance of each adsorption cycle was evaluated by its regenerated adsorption capacity, Q_r (mmol g^{-1}) and regenerated efficiency, η_r (%) which was calculated using Eq. (3):

$$\eta_r(\%) = (Q_r/Q_o) \times 100 \quad (3)$$

where Q_o is the adsorption capacity of the virgin adsorbent (mmol g^{-1}).

RESULTS AND DISCUSSION

1. Adsorbent Synthesis and Characterization

The change in surface morphology of the CP-Pure after being modified with MPTES and RR was observed using scanning electron microscopy (SEM) and is shown in Table 1. The presence of MPTES and RR in the CP-Pure was confirmed using FTIR analysis (Fig. 1). Peaks related to the carbon-linkage and oxygen-linkage groups from lignin, hemicellulose and cellulose were detected on the FTIR spectra of all adsorbents. Additional peaks at 2,600

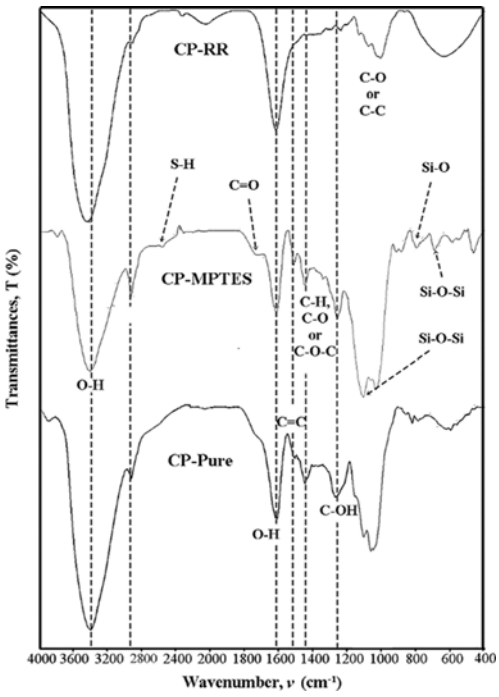

Fig. 1. A comparison of FTIR spectra of CP-Pure and modified CPs (CP-MPTES and CP-RR).

Table 1. Molecular structure of modifying agents and adsorbents characterization

Adsorbents	Modifying agents and molecular structures	Morphology at 1000× magnification	pH_{pzc}	SA ($m^2\ g^{-1}$)	References
CP-Pure	N/A	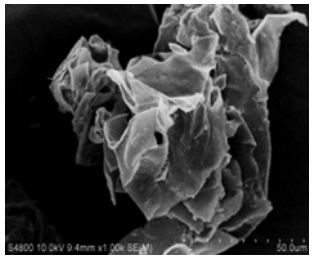	6.25	3.28	[9]
CP-MPTES	3-Mercaptopropyltriethoxysilane 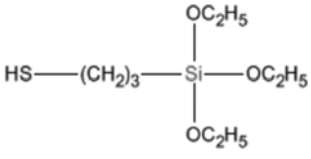	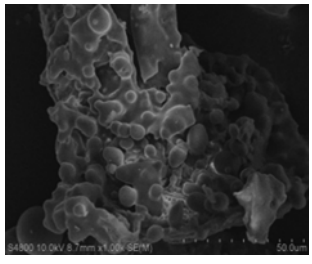	3.28	3.43	[4]
CP-RR	Reactive Red 120 (RR) 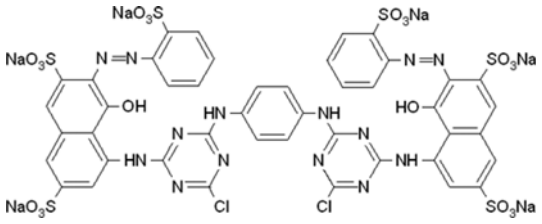	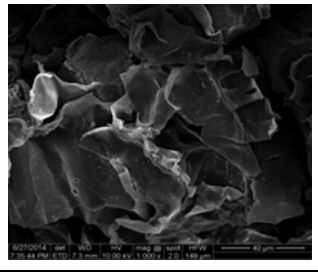	7.65	*N/A	[8]

*BET surface area (SA) of CP-RR cannot be measured using nitrogen adsorption/desorption measurement

Table 2. The breakthrough characteristics and adsorption capacity of Hg(II) and MeHg(II) adsorption onto CP adsorbents in a fixed-bed adsorber at different process conditions

Parameters			Hg(II)					MeHg(II)				
Z (cm)	F (L min^{-1})	C_o (mM)	t_b (min)	$t_{1/2}$ (min)	t_s (min)	$V_{treated}$ (L)	Q_s (mmol g^{-1})	t_b (min)	$t_{1/2}$ (min)	t_s (min)	$V_{treated}$ (L)	Q_s (mmol g^{-1})
(a) CP-Pure								-				
1.0	5	0.25	50	363	1090	5.45	3.92	-	15	240	1.20	0.29
2.0	5	0.25	170	790	1450	7.25	4.09	-	35	365	1.83	0.31
4.0	5	0.25	765	1645	3000	15.00	4.60	-	130	440	2.20	0.45
2.0	1.5	0.25	1710	2650	4600	6.90	4.44	-	250	510	0.77	1.09
2.0	10	0.25	-	220	1080	10.80	3.29	-	-	83	0.83	0.21
2.0	5	0.50	85	370	1440	7.20	5.27	-	25	220	1.10	0.42
2.0	5	1.00	-	270	950	4.75	6.79	-	-	150	0.75	0.45
(b) CP-MPTES												
1.0	5	0.25	10	40	390	1.95	0.66	-	21	300	1.50	0.54
2.0	5	0.25	70	340	1040	5.20	2.14	-	90	500	2.50	0.66
3.8	5	0.25	150	1160	2300	11.50	3.24	-	200	920	4.60	0.74
2.0	1.5	0.25	270	1330	2900	4.35	2.24	-	560	1210	1.82	0.75
2.0	10	0.25	-	75	520	5.20	1.47	-	17	245	2.45	0.43
2.0	5	0.50	-	340	1200	6.00	4.56	-	35	370	1.85	0.75
2.0	5	1.00	-	225	800	4.00	6.37	-	26	230	1.15	0.84
(c) CP-RR												
1.0	5	0.25	90	270	830	4.15	3.38	-	36	150	0.75	0.43
2.0	5	0.25	190	745	2070	10.35	4.53	-	75	390	1.95	0.52
3.8	5	0.25	240	2430	4105	20.53	6.84	-	220	645	3.23	0.55
2.0	1.5	0.25	465	2095	3840	5.76	3.38	-	190	530	0.28	0.32
2.0	10	0.25	2	215	580	5.80	2.86	-	6	185	5.30	0.25
2.0	5	0.50	80	527	1720	8.60	6.49	-	36	330	1.65	0.68
2.0	5	1.00	-	285	1110	5.55	7.64	-	33	190	0.95	0.82

t_b is time when C_t reached 10% of C_o (C_t/C_o=0.1), $t_{1/2}$ is time when C_t reached 50% of C_o (C_t/C_o=0.5), t_s is time when C_t reached 95% of C_o (C_t/C_o=0.95), $V_{treated}$ is the total effluent treated up to t_s and Q_s is the adsorption capacity at exhaustion time

cm^{-1}, 1,010 cm^{-1}, 800 cm^{-1}, and 900 cm^{-1} were detected on the CP-MPTES that correspond to the -SH stretching, Si-O-Si- stretching, symmetrical Si-O-Si-stretching, and Si-O stretching vibrations, respectively. The FTIR spectra of CP-RR have an almost similar pattern with the CP-Pure. Most of the functional groups present in RR such as -NH, N=N, C-S, and S=O cannot be detected using the FTIR as they usually overlapped with other strong vibration linkages like -OH, C=O, C-O, C-C, and C-H.

The CP adsorbents have a relatively low surface area (<4 m^2 g^{-1}); thus the presence of active sites at the adsorbent surfaces became the main factor that affected the adsorption performance. Previous studies on Hg(II) and MeHg(II) adsorption performed in a batch adsorption system proved that the modification of CP using MPTES and RR resulted in a higher adsorption performance than the unmodified CP [4,8,9]. The adsorption mechanism suggests the presence of terminal sulfur group (SH-) from MPTES structure and oxygen (O), nitrogen (N) and sulfur (S) functional groups from RR structure (Table 1) is the main factor for high adsorption towards Hg(II) and MeHg(II). Therefore, a further study on adsorption dynamics was carried out to evaluate the potential application of low-cost reactive agrowaste adsorbents for industrial application.

2. Adsorption Dynamics Parameter Studies

The study on adsorption dynamics of Hg(II) and MeHg(II) on CP adsorbents was performed in a fixed-bed adsorber at various F, C_o, and Z values. The effect of solution feed rate was studied by varying F at (1.5, 5.0 and 10) mL min^{-1}. The increase of F from 1.5 mL min^{-1} to 10 mL min^{-1} resulted in decreasing breakthrough time (t_b) and the saturation time (t_s) (Table 2). At a higher F, the turbulence of flow increased, hence decreasing the mass transfer resistance at adsorbent surfaces, resulting in a faster saturation time [31]. The Q_s decreased with increasing F observed for all cases except for MeHg(II) adsorption onto the CP-RR. At a higher F, the residence time of mercury ions in the adsorber was lower and the mercury might have left the adsorber with incomplete adsorption, hence reducing the adsorption performance.

To evaluate the effect of Z, the adsorber was filled with different amounts of adsorbent (i.e., 0.1 g, 0.2 g and 0.4 g). The C_o and F of the feed solution were fixed at 0.25 mM and 5 mL min^{-1}, respectively. At a higher Z, the t_b and t_s values were longer, the treated volume increased, thus increasing mercury ion adsorption capacity (Table 2). At a shorter Z, the t_s approached faster hence, reducing the adsorption performance [32,33].

Table 3. Adsorption performance of various adsorbents as reported in literature

Adsorbents	Mercury species	F (mL min^{-1})	C_o (mmol g^{-1})	Z (cm)	t_b or V_b	Q_s (mmol g^{-1})	References
ETS-4	Hg(II)	8.45	0.006	8	t_b=148 h	0.17	[35]
DTMAN	Hg(II)	1.0	5.0	-	V_b=160 mL	1.58	[36]
PAN-ATD	Hg(II)	0.25	1.0	-	V_b=130 mL	2.29	[37]
*AC-S	Hg(II)	1	0.25	2	t_b=90 h	1.29	[38]
RSGM	Hg(II)	4.0	0.25	4.5	t_b=120 min	0.83	[7]
MWCNT-AA	Hg(II)	0.7	2.5	5	t_b=31 min	0.51	[39]
MWCNT	Hg(II)	0.7	2.5	5	t_b=17 min	0.16	
SB	Hg(II)	10	0.50	-	t_b~930 min	0.07	[40]
CPN-AP	Hg(II)	0.5	6.0	3	t_b=240 min	1.86	[41]
PUF@PANI	Hg(II)	5.0	0.07	6.7	V_b~600 mL	0.06	[42]
CP-Pure	Hg(II)	5.0	0.25	2	t_b=170 min	4.09	This study
	MeHg(II)	5.0	0.25	2	-	0.31	
CP-MPTES	Hg(II)	5.0	0.25	2	t_b=70 min	2.14	This study
	MeHg(II)	5.0	0.25	2	-	0.66	
CP-RR	Hg(II)	5.0	0.25	2	t_b=190 min	4.53	This study
	MeHg(II)	5.0	0.25	2	-	0.52	

ETS-4=microporous titanosilicate, DTMAN=Dithiocarbamate chelating resin, PAN-ATD=polyacrylonitrile-2-amino-1,3,4-thiadiazole, *AC-S=Thiol-incorporated activated carbon derived from fir wood sawdust, RGSM=rice straw grafted with 3-mercaptopropyltriethoxysilane, MWCNT=multi-walled carbon nanotubes, MWCNT-AA=Amidoamine functionalized multi-walled carbon nanotubes, SB=Spanish broom lignocellulosic sorbent, CPN-AP=chelating resin 2-amino pyridine-functionalized polyacrylonitrile, PUF@PANI=Polyurethane foam-polyaniline

The C_o entering the adsorber is an important parameter since in real field applications the concentration of mercury varies significantly. The effect of C_o was investigated by varying the C_o values at (0.25, 0.50, and 1.0) mM. It was found that the time needed to reach the breakthrough and saturation points was earlier when the C_o increased from 0.25 mM to 1.0 mM. Also, the increase in adsorption capacity is usually achieved with increasing inlet concentration because high C_o would increase the adsorption driving force for the mercury ions adsorption process.

The adsorption capacity (Q_s) of Hg(II) was generally higher than MeHg(II), indicating the higher affinity of the adsorbents towards Hg(II). The present results showed that the CP adsorbents have relatively higher adsorption capacity as compared to other known reported adsorbents (Table 3). The modification of CP using MPTES (CP-MPTES) and RR (CP-RR) showed a substantial improvement towards MeHg(II). This result indicates the functional groups from the MPTES and RR structures provided additional surface active sites for MeHg(II) interaction, thus increasing the Q_s. However, the Hg(II) adsorption using CP-MPTES was surprisingly lower compared to CP-Pure, which contradicts the finding in batch adsorption studies where the organosilane modification can lead to the increase of Hg(II) adsorption [4,34]. Hg(II) adsorption capacity onto CP-MPTES and CP-RR in dynamic system was lower than the batch system in contrast to the MeHg(II). A high adsorption performance in batch system does not guarantee a good dynamic system since the adsorption conditions in both systems are very much different in affecting the removal performance. For instance, the mercury ions and the adsorbent in a batch system were in contact until equilibrium was achieved, while in a continuous adsorption system, solution containing mercury ions continuously passed through the adsorbent bed; thus the composition of adsorbent bed and effluent changed with time.

Although CP-MPTES and CP-RR have a high adsorption capacity towards MeHg(II), their removal performance was lower compared to Hg(II) as the outlet concentration of MeHg(II) even at the earlier stage of adsorption was high (C_t/C_o>0.1). Thus, there were no t_b values observed for the MeHg(II) breakthrough curve, indicating, at the designated conditions, the complete removal of MeHg(II) was impossible. The removal performance can be improved by either lowering feed MeHg(II) concentration or increasing bed height.

3. Isotherm and Kinetic Data Analyses

It was assumed that in a continuous adsorption system, the equilibrium conditions did exist between the adsorbent surfaces and adsorbate in solution at any time t. The concentration of mercury ions at adsorbent surfaces up to time t, q_t is in equilibrium to the concentration of mercury ions in solution at time t, C_t. After saturation (when t>t_s), the effluent concentration should be equal to C_o. Fig. 2 shows the cumulative mercury ions adsorbed per unit adsorbent up to time t, Q_t (mmol g^{-1}) (or mercury ions adsorption capacity) versus mercury concentration in solution at time t, C_t (mmol L^{-1}). The adsorption data were analyzed by using the Langmuir, Freundlich, Dubinin-Radushkevich and Temkin isotherm models. The constant parameters of the models were calculated from the slope and intercept at Y-axis of the linear plot. Table in supplementary information Table S1 shows the linearization isotherm equations and isotherm model parameters of the mercury ion adsorption. The validity of each model was evaluated by comparing the r^2, ARE and MPSD values. The isotherm which has the highest r^2 values and the lowest ARE and MPSD was chosen as the best model to describe the adsorption isotherm data.

The Temkin model was found to fulfill those criteria. To confirm

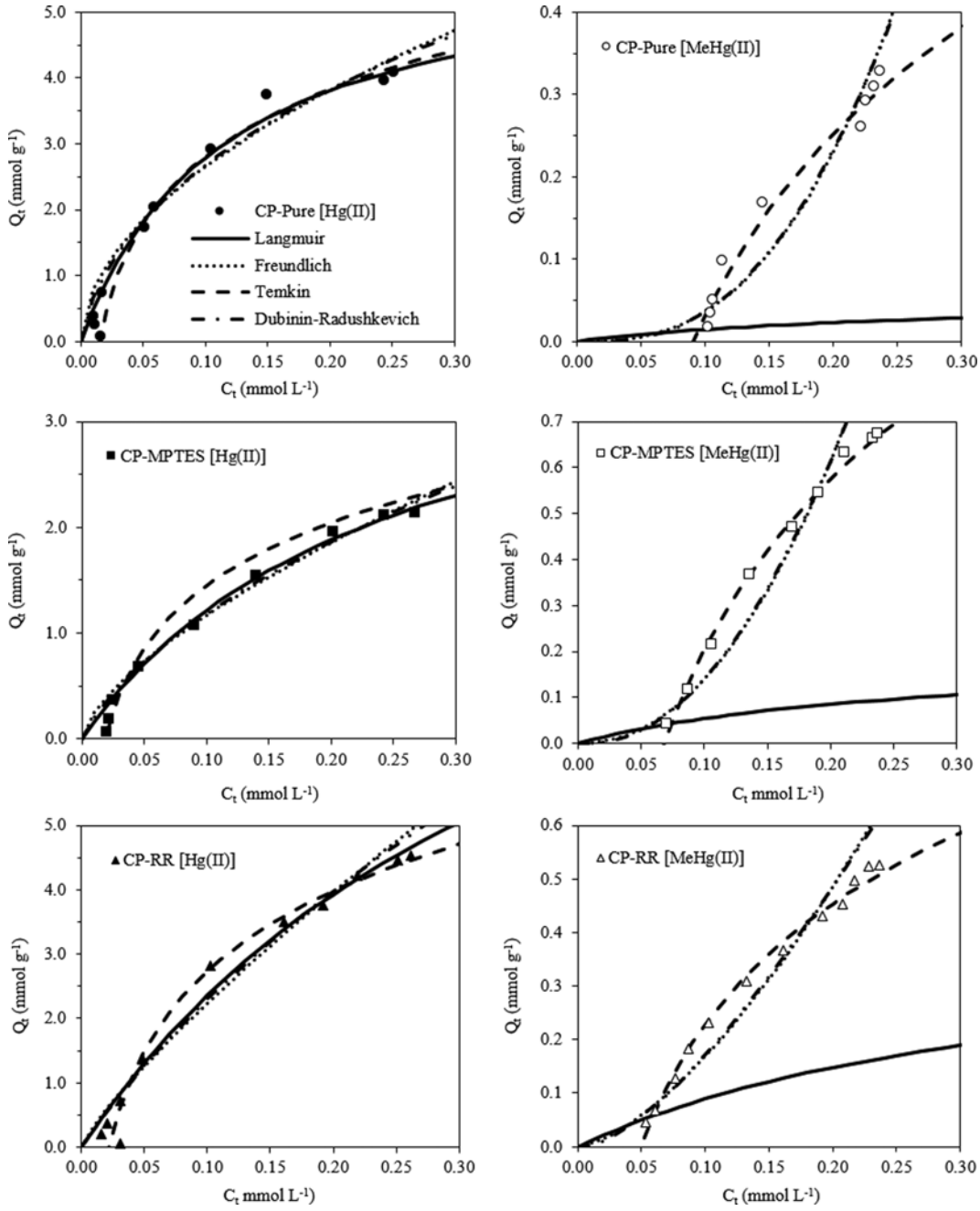

Fig. 2. Comparison between experimental data and isotherm model prediction for continuous Hg(II) and MeHg(II) adsorptions onto CP adsorbents. Experimental conditions: Adsorbent mass, 0.20 g; solution feed flow rate (F), 5 mL min^{-1}; and initial mercury ion concentration (C_o), 0.25 mM.

the results, the experimental data were compared with the model prediction. The constant parameters calculated in Table S1 were used to plot the non-linear isotherm curves by employing the non-linear equations (Fig. 2). The results show that the experimental data of Hg(II) adsorption fitted well with all four isotherms. However, at low C_t, the Langmuir, Freundlich and D-R models deviated from the experimental data. The Temkin isotherm plot of Hg(II) adsorption onto the CP-MPTES fitted well only at lower C_t and the Q_t value was higher than the experimental data for C_t higher than 0.05 mM. In the case of MeHg(II) adsorption onto the CP-Pure and CP-MPTES, the r^2 value of the Temkin model was the highest, while ARE and MPSD values were the lowest compared to other models. The MeHg(II) adsorption onto the CP-RR indicated that the error analysis fitted to the D-R model. However, the value of adsorption capacity estimated from the D-R ($Q_{s,D-R}$) was so much higher than the experimental value (Q_s). The fitting onto Temkin model was closer to the experimental data as compared to other models, observed for all mercury ions adsorption onto the CP adsorbents.

The fitted isotherm in a batch adsorption system for Hg(II) and

MeHg(II) adsorption onto CP-MPTES [4], MeHg(II) adsorption onto the CP-Pure [9] and Hg(II) adsorption onto the CP-RR [8] are different compared to that of the continuous adsorption isotherm. The difference may be due to different assumptions made for the equilibrium conditions. In a batch adsorption, data were collected at equilibrium; therefore, a constant adsorption capacity was achieved. However, in a continuous adsorption, the isotherm analysis was carried out by assuming that the concentration of mercury ion at the adsorbent surface is in equilibrium with the mercury ion concentration in solution at any time t. This assumption may not be true in a continuous adsorption process in which the equilibrium is not achieved since the effluent constantly enters the bed and the system does not have sufficient time to achieve equilibrium.

The cumulative adsorption dynamics data were also analyzed using the existing kinetic models: the pseudo-first order (PFO), pseudo-second order (PSO), Elovich and Fickian models. Table S2 shows the linearization equations of the kinetic models and model parameters of mercury ions adsorption in a fixed-bed adsorber. According to the r^2, ARE and MPSD values, the PSO was the best fitted model to explain the adsorption kinetics. The adsorption capacity estimated from the PSO (Q_{s2}) was higher than the one obtained experimentally (Q_s). The PSO adsorption rate, k_2 of MeHg(II) adsorption onto the CP-Pure and CP-RR was higher than the rate obtained for Hg(II). However, for mercury adsorption onto the CP-MPTES, the k_2 of Hg(II) was higher than the MeHg(II). Fig. 3 shows a good prediction of the PSO kinetic model to the experimental data. This result leads to the conclusion that the PSO kinetic model is suitable to describe the Hg(II) and MeHg(II) adsorption in a dynamic fixed-bed adsorber, which is in accordance with the batch kinetic adsorption studies [4,8,9].

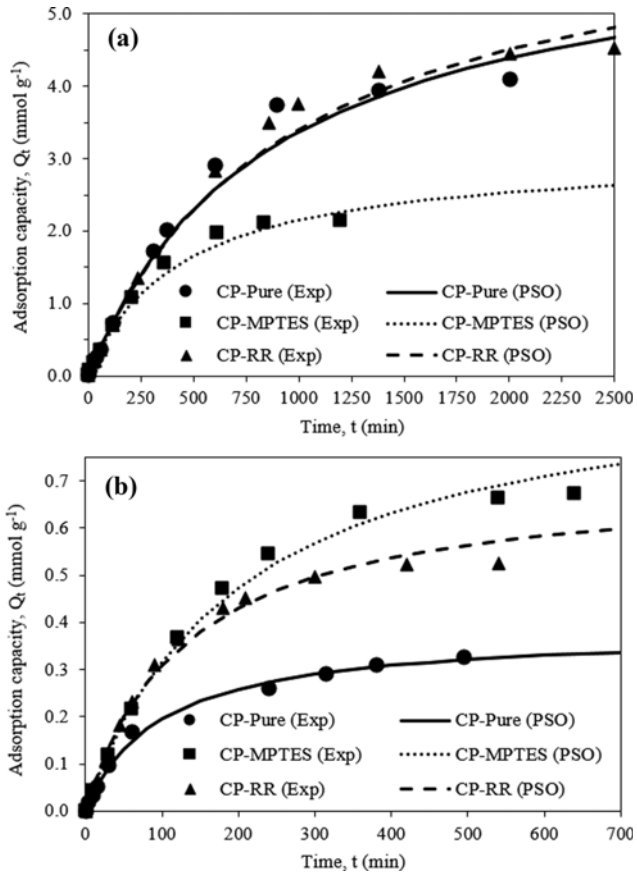

Fig. 3. Comparison between experimental data and pseudo-second order prediction of (a) Hg(II) and (b) MeHg(II) adsorptions onto CP adsorbents.

4. Breakthrough Curves Analysis

In the present study, the well-known breakthrough curve models, the Thomas, Bohart-Adam and Yoon-Nelson, were used to describe the breakthrough curves of the mercury adsorption. The mathematical expressions of the breakthrough models are shown in Table S3.

The Thomas model was developed by assuming that adsorption obeys the PSO reversible kinetics and the Langmuir isotherm [43]. The special feature of the Thomas model is the ability to predict the adsorption capacity, Q_{TH} (or saturated adsorption capacity, Q_s). The Thomas model parameters of both Hg(II) and MeHg(II) adsorption onto CP adsorbents are shown in Table S4. The values of k_{TH} increased and Q_{TH} decreased with increasing F observed for both mercury ions adsorption onto the CP-Pure and CP-MPTES. However, no trend could be seen for both mercury ions adsorption onto the CP-RR. The Q_{TH} also deviated from the experimental data. Since the Thomas model is derived from the PSO kinetic model, which only considers the chemical process mechanism; therefore, it can lead to some errors in determining the adsorption capacity. From the batch adsorption studies, the Hg(II) and MeHg(II) adsorption was found to be a combination of chemical and physical processes [4,8,9].

The Bohart-Adam model was developed based on the surface reaction theory assuming non-instantaneous equilibrium [44]. The model was initially proposed for describing a gas-charcoal adsorption system and then was successfully used for explaining the various adsorption systems [22,32,33]. The values of the Bohart-Adam model parameters of the mercury ions adsorption are given in Table S5. According to the values of r^2, ARE and MPSD, the Bohart-Adam model is not suitable to describe the experimental data.

The Yoon-Nelson model provides the information of 50% adsorber breakthrough [33]. The constants of the Yoon-Nelson model analysis are given in Table S6. The value of k_{YN} increased with F, but it did not show a clear trend towards the effect of C_o and Z. The predicted breakthroughs at 50% (τ), were close to the experimental values ($t_{0.5}$) if the model had a high r^2 value.

The best fitted breakthrough model to describe the breakthrough curves of the adsorption process was evaluated by comparing the values of r^2, ARE and MPSD of the models. It was found that the Thomas and Yoon-Nelson models resulted in the highest r^2 values (i.e., r^2>0.9) and the lowest ARE and MPSD values (Table S4 to Table S6). In addition, the prediction breakthrough curves of the Thomas and Yoon-Nelson models are closer to the experimental data for most adsorption systems (Fig. 4). This confirmed that the models are the most suitable to describe the adsorption dynamics behavior of Hg(II) and MeHg(II).

5. Adsorber Design and Scale-up

The ultimate goal of any adsorption studies is to design and scale-up the process for industrial application, which requires the determination of, among others, the breakthrough curve from the lab-scale experiments as the basis for the prediction of the break-

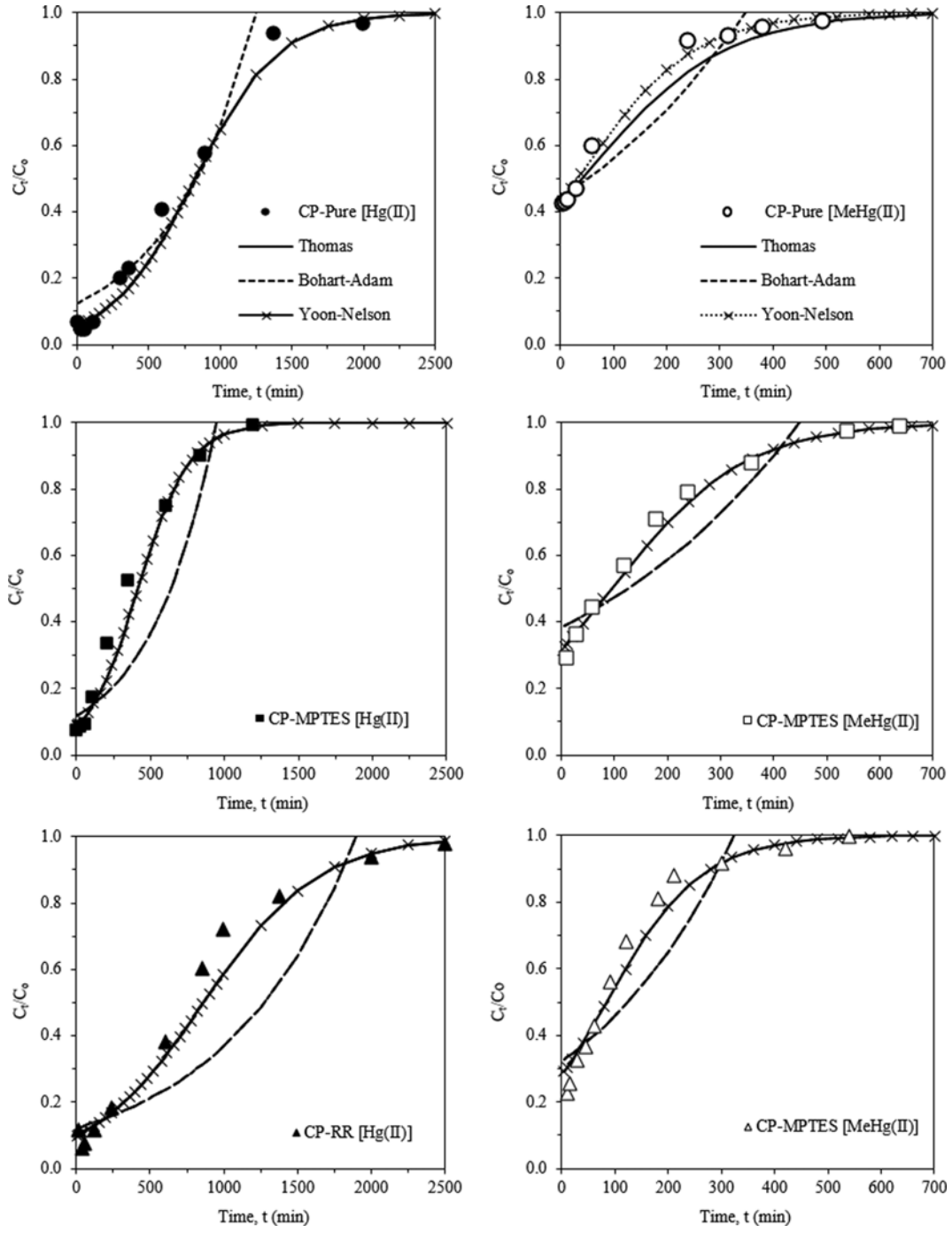

Fig. 4. Comparison of Hg(II) and MeHg(II) adsorption experimental data and breakthrough curves from modelling analysis. Experimental conditions: Adsorbent mass, 0.20 g; solution feed flow rate (F), 5 mL min^{-1}; and initial mercury ion concentration (C_o), 0.25 mM.

through behavior in a full-scale adsorber. The adsorption of Hg(II) and MeHg(II) onto CP-Pure and CP-MPTES, respectively, was used to demonstrate the design and scale-up studies of the adsorption process. This is because both adsorbents showed the highest performance towards both mercury ions. The adsorber design generally requires a detailed consideration of several important parameters as discussed accordingly:

(a) Adsorbent and effluent properties

To design the adsorber for a certain application, the properties of adsorbent and input parameters of the effluent have to be determined. Table 4 shows the properties of adsorbent and adsorbate solution. The important properties of adsorbent include void fraction, average particle diameter and particle density. In the present study, the fluid density and viscosity are assumed to be the same with water properties at 30 °C.

(b) Bed diameter (D)

The bed height to diameter ratio (Z/D) of vertical cylindrical adsorption bed is usually greater than 1.5 [45]. A higher Z/D value

Table 4. Properties of fluid and adsorbent used in the study

Parameters	Values
Particle diameter, $d_p \times 10^3$ (m)	0.875
Void fraction, $\varepsilon_{(CP\text{-}Pure)}$ (dimensionless)	0.405
Void fraction, $\varepsilon_{(CP\text{-}MPTES)}$ (dimensionless)	0.399
Particle density, $\rho_{p\,(CP\text{-}Pure)}$ (g cm^{-3})	0.1316
Particle density, $\rho_{p\,(CP\text{-}MPTES)}$ (g cm^{-3})	0.1180
Fluid density, ρ_f (kg m^{-3})	1.0
Fluid viscosity at 30 °C, $\mu_f \times 10^3$ (Pa·s)	0.798

is necessary especially for the liquid feed to minimize the problem with a large mass transfer zone. In this study, the bed diameter was set at 0.5 m.

(c) Mass of adsorbent (m_{ad})

The amount of adsorbent required to fill up the adsorber can be determined using Eq. (4). The m_{ad} required depends on the density of the adsorbent and volume of the adsorber. The greater adsorbent mass is required for adsorbents which have a high density.

$$m_{ad} = V_{bed} \times \rho_p \tag{4}$$

(d) Empty bed contact time (EBCT)

The EBCT is defined as the relationship between the bed height of the adsorber and the velocity of the feed solution [29]. The relationship can be expressed as Eq. (5).

$$EBCT = Z/v = Z/(F/A) \tag{5}$$

where v is the velocity of the feed solution that relates to the F and cross-sectional area (A) of the adsorber.

(d) Pressure drop

The Ergun equation as given by Eq. (6) is used to determine the pressure drop (ΔP) along the length of the fixed-bed adsorber. According to the Ergun equation, the pressure drop is determined as a function of bed height, adsorbent particle diameter, superficial velocity (υ_o), fluid viscosity, fluid density and void fraction [46].

$$\frac{\Delta P}{Z} = \frac{150\mu_f \upsilon_o (1-\varepsilon)^2}{d_p^2 \varepsilon^2} + \frac{1.75\rho_f \upsilon_o^2 (1-\varepsilon)}{d_p \varepsilon^2} \tag{6}$$

Eq. (6) shows that the ΔP increases with υ_o. The superficial velocity relates to the F of effluent and D of the adsorber. Therefore, at constant D of the adsorber, the ΔP will increase with F. In addition, at the same F, the ΔP across the bed increases if a smaller adsorber diameter is used.

6. Scale-up Adsorber Performance Analysis

6-1. Comparison Between Simulated and Experimental Breakthrough Curves

The adsorption performance of the scale-up adsorber was eval-

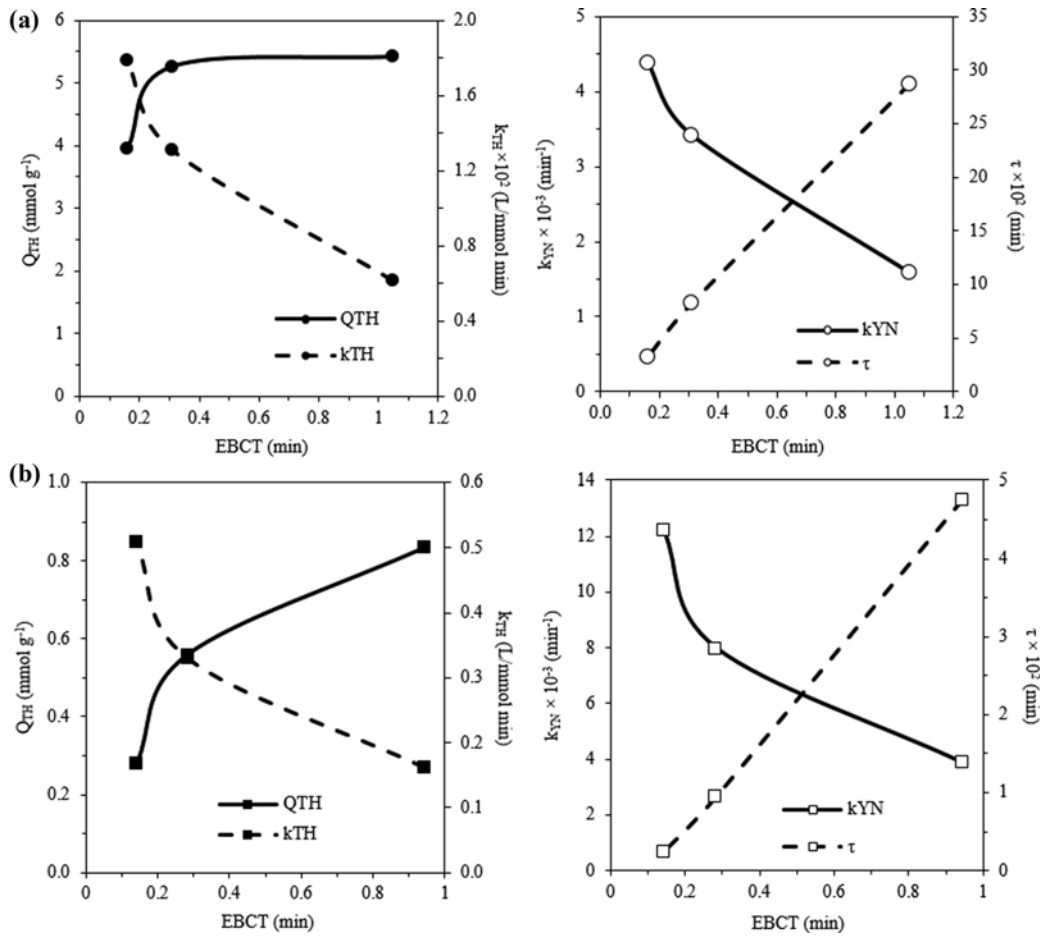

Fig. 5. Thomas and Yoon-Nelson model dependence parameters on the EBCT for (a) CP-Pure-[Hg(II)] and (b) CP-MPTES-[MeHg(II)].

uated based on the breakthrough curve analysis. Since the lab-scale adsorption dynamics data fitted well to the Thomas and Yoon Nelson models, these two models were used to predict the breakthrough curves at different Z values. The F and Z values of the adsorption system were set at 1.5 L min^{-1} to 10 L min^{-1} and 1 cm to 4 cm, respectively.

Fig. 5 shows the Thomas (k_{TH} and Q_{TH}) and the Yoon-Nelson (k_{YN} and τ) parameters plots at different EBCT values. These plots were used to evaluate the new values of k_{TH}, Q_{TH}, k_{YN} and τ at new Z. The values of constant parameters for a new EBCT are given in Table 5. These constants were inserted in the Thomas and the Yoon-Nelson equations so that the breakthrough curves at different Z (i.e., new EBCT) could be plotted. The efficiency of both models was established by comparing the experimental data with the

Table 5. Parameters of Thomas and Yoon-Nelson models evaluated from Fig. 5

Hg(II)	Models	Parameters	Z=1 cm F=5 mL min^{-1} EBCT=0.16 min	Z=4 cm F=5 mL min^{-1} EBCT=0.63 min
	Thomas	$k_{TH}\times10^2$ (L $mmol^{-1}$ min^{-1})	1.78	0.98
		Q_{TH} (mmol g^{-1})	3.95	5.40
	Yoon-Nelson	$k_{YN}\times10^3$ (min^{-1})	4.36	2.60
		τ (min)	318.18	1712.12
MeHg(II)	Models	Parameters	Z=1 cm F=5 mL/min EBCT=0.16 min	Z=3.6 cm F=5 mL/min EBCT=0.57 min
	Thomas	$k_{TH}\times10^2$ (L $mmol^{-1}$ min^{-1})	4.80	2.50
		Q_{TH} (mmol g^{-1})	0.33	0.69
	Yoon-Nelson	$k_{YN}\times10^3$ (min^{-1})	11.48	0.60
		τ (min)	35	262.5

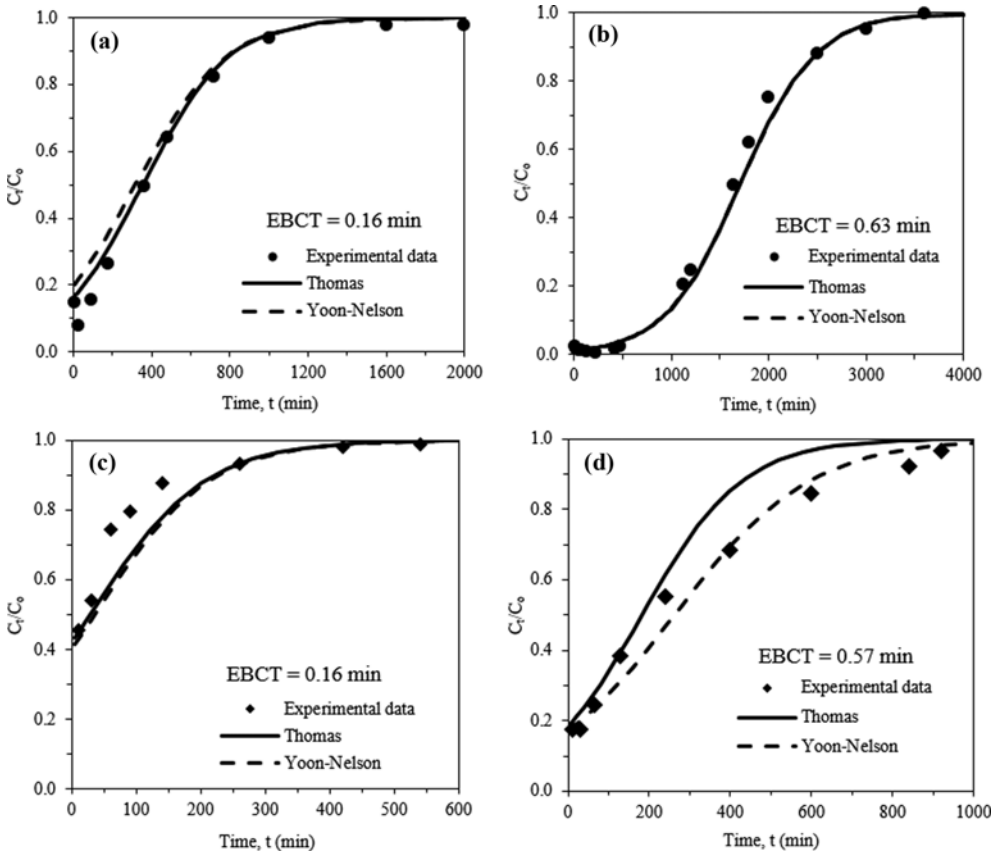

Fig. 6. Comparison of predicted and experimental breakthrough curves of (a), (b) CP-Pure-[Hg(II)] and (c), (d) CP-MPTES-[MeHg(II)] for different EBCT values.

predicted curves. Fig. 6 shows the comparison of breakthrough curve of Hg(II) adsorption at EBCT of 0.16 min and 0.63 min; and MeHg(II) adsorption at EBCT of 0.16 min and 0.57 min. The predicted curves of the Thomas and the Yoon-Nelson models show a good fit for Hg(II) adsorption data observed for both EBCT values. For the MeHg(II) adsorption, at EBCT of 0.16 min, the Thomas and the Yoon-Nelson prediction curves had a similar pattern. However, at EBCT of 0.57 min, the prediction curves by the Yoon-Nelson model are closer to the experimental data compared to the curves obtained from the Thomas model. The EBCT was thus used for the adsorber design and scale-up. To have a good fitting of the experimental curves, the EBCT value should be in the experimentally confirmable range. At constant C_o and Z, the Yoon-Nelson model showed an excellent agreement with the corresponding experimental curves observed for various Z and F values. Thus, it was applied for breakthrough curve simulation of the scale-up adsorber.

6-2. Breakthrough Curves of Scale-up Adsorber

A satisfactory fitting can be achieved when the values of EBCT are in the experimentally confirmable range [30,46]. The EBCT value can be maintained in the experimental range by arbitrarily selecting the Z and F values, while keeping the adsorber diameter (D) constant. In this study, the D of the adsorber was set at 0.5 m. By increasing F of 50 $m^3 h^{-1}$ to 200 $m^3 h^{-1}$, the EBCT values were varied in the range of 0.71 min to 0.18 min and 0.94 min to 0.18 min, for Z of 3 m and 4 m, respectively. The adsorber design parameters and breakthrough properties of the Hg(II) and MeHg(II) adsorption are summarized in Table 6. The υ_o and ΔP, however, were found to increase with F.

The breakthrough curve simulations of Hg(II) and MeHg(II) adsorption in the scale-up adsorber were constructed using the Yoon-Nelson model. The Yoon-Nelson constants at various EBCT values of the scale-up adsorber were determined from the plot of k_{YN} and τ versus EBCT (Fig. 5) and are shown in Table 6. Fig. 7 shows the simulated breakthrough curves of (a) Hg(II) and (b) MeHg(II) adsorption for Z of 3 m and 4 m at varied F values ranging from 50 $m^3 h^{-1}$ to 200 $m^3 h^{-1}$, respectively.

7. Regeneration Studies

In batch adsorption studies, the HCl-regenerated CP-RR showed a high adsorption performance towards Hg(II), while the KI-regener-

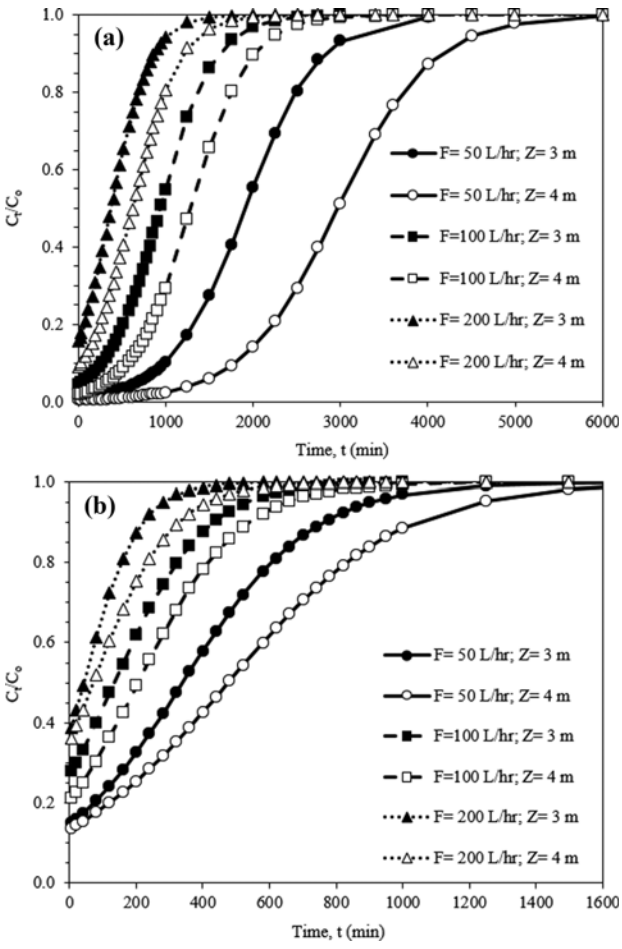

Fig. 7. Prediction breakthrough curves of (a) Hg(II) adsorption onto CP-Pure and (b) MeHg(II) adsorption onto CP-MPTES for a scale-up adsorber.

Table 6. Adsorber design parameters and breakthrough curve parameters of Hg(II) and MeHg(II) adsorption onto CP adsorbents in a scale-up adsorber

Mercury species	Z (m)	D (m)	V_{bed} (m^3)	F ($m^3 h^{-1}$)	v (m h^{-1})	EBCT (min)	m_{ad} (kg)	ΔP (kPa)	$k_{YN}\times10^3$ (min)	τ (min)	t_b (min)	$t_{0.5}$ (min)	t_s (min)
Hg(II)	3	0.5	0.59	50	254.61	0.71	77.53	71.60	2.40	1909.09	1000	960	3200
				100	509.23	0.35		143.35	3.30	939.4	2800	940	1830
				200	1018.56	0.18		286.98	4.50	378.8	n/a	480	1030
	4	0.5	0.79	50	254.61	0.94	103.4	95.50	1.87	2969.7	1580	2598	4750
				100	509.23	0.47		191.08	3.05	1287.9	558	1300	2340
				200	1018.56	0.24		382.45	3.70	621.2	30	620	1420
MeHg(II)	3	0.5	0.59	50	254.61	0.71	70.04	71.60	5.20	339.47	n/a	40	285
				100	509.23	0.35		143.35	7.40	134.21	n/a	135	540
				200	1018.56	0.18		286.98	1.23	42.11	n/a	340	915
	4	0.5	0.79	50	254.61	0.94	93.39	95.50	3.90	476.32	n/a	70	420
				100	509.23	0.47		191.08	6.60	205.26	n/a	207	660
				200	1018.56	0.24		382.45	8.60	71.05	n/a	475	1235

Table 7. Regenerated adsorption capacity, Q_r (mmol g^{-1}) and regenerated efficiency, η_r (%) of Hg(II) and MeHg(II) adsorption in multi-adsorption cycles

Cycle no.	Q_r (mmol g^{-1})	η_r (%)	Q_r (mmol g^{-1})	η_r (%)
(a) Hg(II)	CP-Pure		CP-RR	
1*	4.930	100.00	6.206	100.00
2	3.726	75.58	1.077	17.36
3	2.523	51.18	0.968	15.60
4	1.726	35.01	0.516	8.31
5	1.327	26.92	n/a	n/a
(b) MeHg(II)	CP-Pure		CP-MPTES	
1*	0.405	100.00	0.499	100.00
2	0.396	97.67	0.464	92.74
3	0.368	90.97	0.461	92.22
4	0.301	74.32	0.300	59.91
5	0.188	46.43	0.132	26.43

*Q_r is equal to Q_o for the fresh adsorbent

ated CP-MPTES for MeHg(II). Thus, these two systems were selected for reusability studies in a dynamic adsorption system. The regenerated adsorption capacity (Q_r) and regenerated efficiency (η_r) of Hg(II) and MeHg(II) adsorption using regenerated adsorbents are shown in Table 7.

In general, the adsorption performance of the regenerated adsorbents decreased after each desorption cycle. The η_r of Hg(II) adsorption onto regenerated CP-Pure gradually decreased from 75.58% at second adsorption cycle to 26.92% at fifth adsorption cycle. Although a higher adsorption capacity of the fresh CP-RR towards Hg(II) was observed, the regenerated CP-RR showed a lower adsorption performance than CP-Pure. The Q_r of Hg(II) at the second adsorption cycle decreased of 82.6% and kept decreasing for the subsequent adsorption cycles. This result might be due to the strong chemical interaction between Hg(II) and active sites of the CP-RR, indicating the use of 0.1 M HCl solution was not strong enough to promote desorption of Hg(II) from CP-RR in a dynamic adsorption system. It was confirmed that after eluting with 3.0 L of HCl, only a small amount of Hg(II)-loaded CP-RR was released into the eluent solution observed for all desorption cycles (Fig. 8). The desorption performance could be increased by using a higher acid concentration because it can provide more exchangeable H^+ ions with metal ions [22].

The regenerated MeHg(II)-loading adsorbents using KI showed a stable adsorption performance up to the third adsorption cycle, with the η_r of higher than 90%. After the first cycle of desorption process, only half of the MeHg(II)-loaded in both CP-Pure and CP-MPTES was released to the eluent solution (Fig. 8), indicating that some of the active sites have stronger binding with MeHg(II) and cannot be desorbed. After multiple adsorption-desorption activities, the available active sites for MeHg(II) adsorption become limited due to the accumulation of MeHg(II), thus lowering the adsorption efficiency of regenerated adsorbent afterwards. The different MeHg(II) desorption capacity of CP-Pure and CP-MPTES was due to the difference in active sites involved in the MeHg(II)

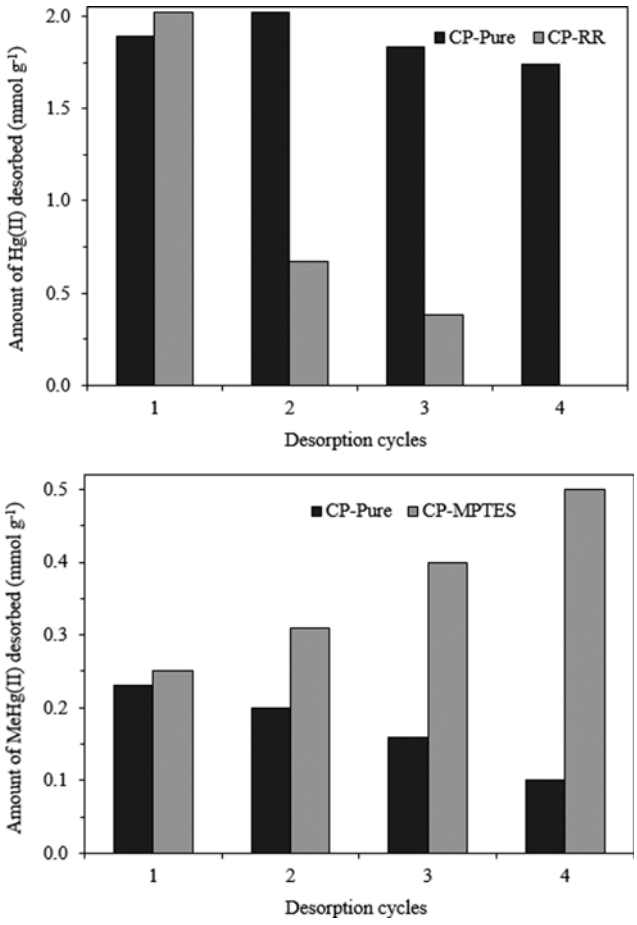

Fig. 8. Desorption capacity of Hg(II) and MeHg(II) after multiple adsorption cycles in which HCl and KI solutions were used as desorption agents, respectively.

adsorption onto both adsorbents.

CONCLUSIONS

Adsorption dynamics analysis of Hg(II) and MeHg(II) on low-cost adsorbents of CP-Pure, CP-MPTES and CP-RR was conducted in a fixed-bed adsorber performed at various Z, F, and C_o values. The adsorption capacity of Hg(II) was greater than MeHg(II) observed for all adsorbents even though its adsorption capacity of MPTES is slightly lower than CP-Pure. The MeHg(II) adsorption capacity of CP-MPTES and CP-RR showed substantial improvement as compared to CP-Pure. The adsorption isotherm and kinetic model indicated that the adsorption data fitted well to the Temkin isotherm and pseudo-second order kinetic models, respectively. The breakthrough curves of mercury ion adsorption at the studied conditions mostly fitted the Thomas and the Yoon-Nelson models, which were then applied to predict the breakthrough curves of a scale-up adsorber. The scale-up adsorber was designed based on the EBCT concept. The Yoon-Nelson model shows excellent agreement with the experimental breakthrough curves of Hg(II) and MeHg(II) adsorption operated at various operating variables of F and Z. The KI-regenerated adsorbent showed a high regeneration

efficiency up to the third MeHg(II) cycle of adsorption, in contrast a lower Hg(II) regeneration efficiency of the HCl-regenerated adsorbent was observed.

ACKNOWLEDGEMENTS

The financial support from the Universiti Teknologi Malaysia for Research University Grant (GUP 15H77) and Postdoctoral Fellowship Scheme (PDRU 04E29 and PDRU 03E92) awarded to Norasikin Saman and Safia Syazana Mohtar and the Ministry of Higher Education (MOHE) Malaysia for MyBrain15 scholarship are gratefully acknowledged.

SUPPORTING INFORMATION

Additional information as noted in the text. This information is available via the Internet at http://www.springer.com/chemistry/journal/11814.

REFERENCES

1. B. Jimenez Cisneros and J. B. Rose, *Urban Water Security: Managing Risks*, 2009, London, CRC Press.
2. W. Marimón-Bolívar, L. Tejeda-Benítez and A. P. Herrera, *Environ. Nanotech. Monitor. Manag.*, **10**, 486 (2018).
3. P. Balderas-Hernández, G. Roa-Morales, M. T. Ramírez-Silva, M. Romero-Romo, E. Rodríguez-Sevilla, J. M. Esparza-Schulz and J. Juárez-Gómez, *Chemosphere*, **167**, 314 (2017).
4. N. Saman, K. Johari, S.-T. Song, H. Kong, S.-C. Cheu and H. Mat, *Chemosphere*, **171**, 19 (2017).
5. N. Saman, K. Johari, S.-T. Song and H. Mat, *Environ. Earth Sci.*, **75**, 345 (2016).
6. K. Johari, N. Saman, S. T. Song, S. C. Cheu, H. Kong and H. Mat, *Chemosphere*, **156**, 56 (2016).
7. S.-T. Song, Y.-F. Hau, N. Saman, K. Johari, S.-C. Cheu, H. Kong and H. Mat, *J. Environ. Chem. Eng.*, **4**, 1685 (2016).
8. N. Saman, K. Johari, S.-T. Song, H. Kong, S.-C. Cheu and H. Mat, *Environ. Prog. Sustain. Energy*, **38**, S54 (2019).
9. N. Saman, K. Johari, S.-T. Song, H. Kong, S.-C. Cheu and H. Mat, *J. Environ. Chem. Eng.*, **4**, 2487 (2016).
10. A. Teimouri, H. Esmaeili, R. Foroutan and B. Ramavandi, *Korean J. Chem. Eng.*, **35**, 479 (2018).
11. S. Zarei and M. Niad, *J. Taiwan. Inst. Chem. Eng.*, **81**, 247 (2017).
12. M. Hadavifar, N. Bahramifar, H. Younesi, M. Rastakhiz, Q. Li, J. Yu and E. Eftekhari, *J. Taiwan. Inst. Chem. Eng.*, **67**, 397 (2016).
13. J.-H. Park, J. J. Wang, B. Zhou, J. E. R. Mikhael and R. D. DeLaune, *Environ. Poll.*, **244**, 627 (2019).
14. Q. Zhou, Y. Duan, C. Zhu, J. Zhang, M. She, H. Wei and Y. Hong, *Korean J. Chem. Eng.*, **32**, 1405 (2015).
15. S. Kushwaha and P. P. Sudhakar, *Carbohyd. Polym.*, **86**, 1055 (2011).
16. O. S. Akintola, T. A. Saleh, M. M. Khaled and O. C. S. Al Hamouz, *J. Taiwan. Inst. Chem. Eng.*, **60**, 602 (2016).
17. M.-J. López-Muñoz, A. Arencibia, L. Cerro, R. Pascual and Á. Melgar, *Appl. Surf. Sci.*, **367**, 91 (2016).
18. N. Saman, K. Johari and H. Mat, *Ind. Eng. Chem. Res.*, **53**, 1225 (2014).
19. N. Saman, K. Johari and H. Mat, *Micropor. Mesopor. Mater.*, **194**, 38 (2014).
20. Ş. Yılmaz, T. Şahan and A. Karabakan, *Korean J. Chem. Eng.*, **34**, 2225 (2017).
21. M. A. K. M. Hanafiah, H. Zakaria and W. S. W. Ngah, *CLEAN - Soil, Air, Water*, **38**, 248 (2010).
22. J. Goel, K. Kadirvelu, C. Rajagopal and V. Kumar Garg, *J. Hazard. Mater.*, **125**, 211 (2005).
23. R. A. Hutchins, *Chem. Eng.*, **80**, 133 (1973).
24. P. Suksabye, P. Thiravetyan and W. Nakbanpote, *J. Hazard. Mater.*, **160**, 56 (2008).
25. R. Han, Y. Wang, X. Zhao, Y. Wang, F. Xie, J. Cheng and M. Tang, *Desalination*, **245**, 284 (2009).
26. K. S. Rao, S. Anand and P. Venkateswarlu, *J. Ind. Eng. Chem.*, **17**, 174 (2011).
27. Q. Yang, Y. Zhong, X. Li, X. Li, K. Luo, X. Wu, H. Chen, Y. Liu and G. Zeng, *J. Ind. Eng. Chem.*, **28**, 54 (2015).
28. M. Abdelmouleh, S. Boufi, M. N. Belgacem, A. P. Duarte, A. Ben Salah and A. Gandini, *Int. J. Adhes. Adhes.*, **24**, 43 (2004).
29. N. V. Medvidović, J. Perić and M. Trgo, *Sep. Purif. Technol.*, **49**, 237 (2006).
30. M. Trgo, N. V. Medvidović and J. Perić, *Indian J. Chem. Technol.*, **18**, 123 (2011).
31. M. Karimi, A. Shojaei, A. Nematollahzadeh and M. J. Abdekhodaie, *Chem. Eng. J.*, **210**, 280 (2012).
32. X. Xu, B. Gao, X. Tan, X. Zhang, Q. Yue, Y. Wang and Q. Li, *Chem. Eng. J.*, **226**, 1 (2013).
33. A. P. Lim and A. Z. Aris, *Biochem. Eng. J.*, **87**, 50 (2014).
34. S.-T. Song, N. Saman, K. Johari and H. Mat, *Environ. Prog. Sustain. Energy*, **34**, 1298 (2015).
35. C. Lopes, E. Pereira, Z. Lin, P. Pato, M. Otero, C. Silva, J. Rocha and A. Duarte, *Micropor. Mesopor. Mater.*, **145**, 32 (2011).
36. A. Shaaban, D. Fadel, A. Mahmoud, M. Elkomy and S. Elbahy, *J. Environ. Chem. Eng.*, **1**, 208 (2013).
37. C. Xiong, Y. Li, G. Wang, L. Fang, S. Zhou, C. Yao, Q. Chen, X. Zheng, D. Qi and Y. Fu, *Chem. Eng. J.*, **259**, 257 (2015).
38. F. Kazemi, H. Younesi, A. A. Ghoreyshi, N. Bahramifar and A. Heidari, *Process Saf. Environ. Prot.*, **100**, 22 (2016).
39. A. S. Deb, V. Dwivedi, K. Dasgupta, S. M. Ali and K. Shenoy, *Chem. Eng. J.*, **313**, 899 (2017).
40. F. E. A. Arias, A. Beneduci, F. Chidichimo, E. Furia and S. Straface, *Chemosphere*, **180**, 11 (2017).
41. S. M. El-Bahy and Z. M. El-Bahy, *J. Environ. Chem. Eng.*, **5**, 3560 (2017).
42. S. A. Vali, M. Baghdadi and M. A. Abdoli, *J. Environ. Chem. Eng.*, **6**, 6612 (2018).
43. H. C. Thomas, *J. Am. Chem. Soc.*, **66**, 1664 (1944).
44. G. S. Bohart and E. Q. Adams, *J. Am. Chem. Soc.*, **42**, 523 (1920).
45. A. P. Shinha and D. Parameswar, *Mass Transfer: Principle and Operations*, New Delhi, India: PHI Learning Private Limited (2012).
46. J. K. B. Schnelle and C. A. Brown, *Air Pollution Control Technology Handbook*, CRC Press, Boca Raton, Florida (2001).

Supporting Information

A comparative study on dynamic Hg(II) and MeHg(II) removal by functionalized agrowaste adsorbent: breakthrough analysis and adsorber design

Norasikin Saman[*], Helen Kong[**], Safia Syazana Mohtar[*], Khairiraihanna Johari[***], Azmi Fadziyana Mansor[*], Onn Hassan[*], Noorhalieza Ali[*], and Hanapi Mat[*,**,†]**

*Advanced Materials and Process Engineering Laboratory, School of Chemical and Energy Engineering, Faculty of Engineering, Universiti Teknologi Malaysia, 81310 UTM Skudai, Johor, Malaysia
**Centre of Lipid Engineering and Applied Research, Level 2, Block C08, Faculty of Science, Universiti Teknologi Malaysia, Universiti Teknologi Malaysia, 81310 UTM Skudai, Johor, Malaysia
***Department of Chemical Engineering, Faculty of Engineering, Universiti Teknologi PETRONAS, 32610, Bandar Seri Iskandar, Perak, Malaysia
****Advanced Materials and Separation Technologies (AMSET) Research Group, Health and Wellness Research Alliance, Universiti Teknologi Malaysia, 81310 UTM Skudai, Johor, Malaysia
(*Received 7 November 2018 • Accepted 27 April 2019*)

Table S1. Isotherm parameters of Hg(II) and MeHg(II) adsorption in a fixed-bed adsorber

Adsorbents	CP-Pure		CP-MPTES		CP-RR	
Parameters	Hg(II)	MeHg(II)	Hg(II)	MeHg(II)	Hg(II)	MeHg(II)
Q_s	4.089	0.310	2.138	0.663	4.525	0.524
Langmuir: $C_t/Q_t=1/Q_{s,L}b+C_t/Q_{s,L}$						
$Q_{s,L}$ (mmol g^{-1})	5.989	0.053	4.165	0.202	11.854	0.435
b (L $mmol^{-1}$)	8.724	3.8108	4.126	3.651	2.480	2.568
r^2	0.9763	0.4272	0.9783	0.5007	0.7980	0.4403
ARE	135.0793	74.9703	60.8014	71.2000	144.0019	54.9792
MPSD	412.9220	89.7361	165.7337	86.0799	455.8989	63.8238
Freundlich: $\ln Q_t=\ln k_f+1/n \ln C_t$						
k_f ($L^n mol^{1-n} g^{-1}$)	2.969	1501537	1.780	52000	4.480	214
n	1.901	0.377	1.491	0.467	1.211	0.655
r^2	0.9455	0.8228	0.9922	0.9278	0.9676	0.9405
ARE	205.9232	33.2031	82.5844	22.2901	148.8177	17.0868
MPSD	577.4070	56.0655	217.9573	31.1415	458.0527	21.8607
Dubinin-Radushkevich (D-R): $\ln Q_t=\ln Q_{s,D-R}-2\beta_{D-R}\varepsilon^2$, where $\varepsilon=RT \ln (1-1/C_t)$						
$Q_{s,D-R}$ (mmol g^{-1})	31.742	13992	27.133	3780	101.673	222
$-\beta_{D-R}\times10^9$ (J mol^{-1})	4.588	23.881	5.810	18.931	7.034	13.295
E_{D-R} (kJ mol^{-1})	10.439	4.576	9.277	5.139	8.431	6.133
r^2	0.9548	0.8274	0.9941	0.9363	0.9764	0.9491
ARE	179.6292	32.5803	72.5909	20.8420	140.5110	7.1805
MPSD	516.286	54.9870	194.2031	28.8478	442.9201	14.4275
Temkin: $Q_t=(RT/b_T) \ln A_T+(RT/b_T) \ln C_t$						
$b_T\times10^{-3}$ (kJ mol^{-1})	1.712	7.899	2.939	4.697	1.400	7.743
$A_T\times10^{-4}$ (L mol^{-1})	6.735	1.102	5.433	1.460	4.566	2.016
r^2	0.9683	0.9774	0.9830	0.9933	0.9960	0.9920
ARE	77.2571	24.1084	14.7973	11.1596	137.4957	15.6240
MPSD	141.6787	51.6283	19.4815	26.7816	354.7534	19.9784

Experimental conditions: Adsorbent mass, 0.20 g; feed solution flow rate, 5 mL min^{-1} and initial mercury ion concentration, 25 mM

Table S2. Kinetic model constants of Hg(II) and MeHg(II) adsorption in a fixed-bed adsorber

Adsorbents	CP-Pure		CP-MPTES		CP-RR	
Mercury ions	Hg(II)	MeHg(II)	Hg(II)	MeHg(II)	Hg(II)	MeHg(II)
$Q_{s.exp}$ (mmol g^{-1})	4.089	0.310	2.135	0.663	4.525	0.524
Pseudo-first order (PFO): $\ln (Q_s - Q_t) = \ln Q_{s1} - k_1 t$						
Q_{s1} (mmol g^{-1})	4.153	0.402	3.998	1.588	6.043	1.534
$k_1 \times 10^3$ (min^{-1})	1.979	15.531	7.178	15.263	2.468	23.208
r^2	0.9818	0.7714	0.9182	0.8739	0.9560	0.7642
ARE	13.5699	49.9306	203.2457	252.7429	81.9966	352.2839
MPSD	20.0993	59.9934	257.0601	312.5533	102.3770	416.4081
Pseudo-second order (PSO): $t/Q_t = 1/(k_2 Q_e^2) + (1/Q_{s2})t$						
Q_{s2} (mmol g^{-1})	6.316	0.383	3.079	0.943	6.648	0.709
$k_2 \times 10^3$ (mmol min^{-1})	0.181	27.097	0.752	5.361	0.158	10.928
r^2	0.9522	0.9943	0.9715	0.9880	0.9715	0.9902
ARE	8.9912	5.3012	7.3641	5.0780	7.8391	5.3804
MPSD	11.38858	7.5968	9.4769	6.2323	10.1013	7.0434
Elovich: $Q_t = (1/\beta)\ln(\alpha\beta) + (1/\beta)\ln t$						
β (g $mmol^{-1}$)	1.118	13.968	1.983	5.789	1.035	7.056
α (mmol g^{-1} min^{-1})	0.036	0.012	0.028	0.015	0.037	0.015
r^2	0.9006	0.9835	0.9363	0.9622	0.9195	0.9811
ARE	104.3401	43.0263	70.7180	36.2999	106.5323	30.8540
MPSD	185.3602	78.4568	129.2583	71.9119	195.0642	56.1220
Fickian's diffusion: $\frac{Q_t}{Q_e} = 1 - \frac{6}{\pi^2}\sum_{n-1}^{\infty}\frac{1}{n^2}\exp\left(\frac{-n^2\pi^2 D_{eff} t}{R_p^2}\right)$						
$D_{eff} \times 10^{11}$ (cm^2 min^{-1})	5.679	45.980	0.222	47.053	7.323	9.290
$K_{fd} \times 10^3$ (min^{-1})	1.757	14.229	6.859	14.561	2.266	2.875
r^2	0.9502	0.6913	0.8835	0.8118	0.8847	0.9456
ARE	379.7439	142.7357	228.6995	105.8646	414.0309	83.8428
MPSD	930.3954	261.5349	511.0865	210.0281	1024.1269	138.2091

Experimental conditions: Adsorbent mass, 0.20 g; feed solution flow rate, 5 mL min^{-1} and initial mercury ion concentration, 25 mM

Table S3. Mathematical expressions of common breakthrough curve model analysis

Models	Non-linear and linear mathematical expressions	Remarks
Thomas	$C_t/C_o = 1/1 + \exp(k_{Th}/F(Q_{TH}m - C_o V_{eff}))$ $\ln[(C_o/C_t) - 1] = (k_{TH}Q_{TH}m/F) - (k_{TH}C_o V_{eff}/F)$	k_{TH} is the Thomas rate constant (mL $mmol^{-1}$ min^{-1}), Q_{TH} is the adsorption capacity (mmol g^{-1}), m is the amount of adsorbent (g), V_{eff} is the volume of effluent (L) and F is the flow rate of effluent (mL min^{-1}).
Bohard-Adam	$Ct/Co = \exp[kBACot - kBANo(Z/v)]$ $\ln(C_t/C_o) = k_{BA}C_o t - k_{BA}N_o(Z/v)$	N_o is the saturation concentration (mmol L^{-1}), Z is the bed height of the column (cm), k_{BA} is the rate constant of the Bohart-Adam model (L $mmol^{-1}$ min^{-1}), and v is the linear flow rate (cm min^{-1}) which is related to the diameter of the adsorber (v=F/A), A is cross-sectional area of adsorber.
Yoon-Nelson	$C_t/C_o = [\exp(k_{YN}(t - \tau))]/[\exp(k_{YN}(t - \tau)]$ $\ln(C_t/(C_o - C_t)) = tk_{YN} - \tau k_{YN}$	k_{YN} is the Yoon-Nelson constant (min^{-1}) and τ is the time required to achieve 50% breakthrough (min).

Table S4. Thomas model parameters of Hg(II) and MeHg(II) adsorption onto CP adsorbents at different Z, F and C_o

Samples	F	C_o	Z	$k_{TH}\times10^2$	Q_{TH}	$Q_{s.exp}$	r^2	ARE	MPSD
Hg(II) adsorption									
CP-Pure	1.5	0.25	2.0	0.615	5.420	4.443	0.8241	113.9348	232.6258
	5	0.25	2.0	1.310	5.261	4.089	0.9602	22.7061	33.6931
	10	0.25	2.0	1.675	4.101	3.298	0.9070	18.1828	22.8828
	5	0.50	2.0	0.702	8.170	5.266	0.8307	21.3278	33.1688
	5	1.00	2.0	0.210	2.410	6.791	0.8705	12.2254	18.4180
	5	0.50	1.0	1.225	5.330	3.919	0.8999	29.1388	55.6362
	5	0.50	4.0	1.066	5.232	4.604	0.9289	9.1219	21.4960
CP-MPTES	1.5	0.25	1.8	0.933	2.806	2.240	0.9249	76.4737	199.2182
	5	0.25	1.8	2.105	2.708	2.138	0.9864	14.3594	20.5075
	10	0.25	1.8	3.202	1.378	1.467	0.9671	46.3125	61.6142
	5	0.50	1.8	0.778	4.864	4.561	0.9881	24.8583	33.7077
	5	1.00	1.8	0.494	5.921	6.366	0.9449	7.1213	12.1675
	5	0.50	1.0	3.958	0.874	0.657	0.8126	36.720	81.838
	5	0.50	3.6	0.952	3.844	3.242	09742	57.6497	70.0957
CP-RR	1.5	0.25	1.9	0.629	4.120	3.379	0.9580	33.1338	69.5983
	5	0.25	1.9	0.964	5.688	4.525	0.9724	18.8294	31.5746
	10	0.25	1.9	2.959	3.109	2.856	0.9848	6.4237	8.0109
	5	0.50	1.9	0.676	8.749	6.489	0.9473	26.3301	47.4342
	5	1.00	1.9	0.417	9.735	7.644	0.9802	29.2198	38.5606
	5	0.50	1.0	2.470	6.432	3.381	0.8523	64.3811	97.2623
	5	0.50	3.8	4.932	7.051	6.844	0.9376	6.5576	11.1747
MeHg(II) adsorption									
CP-Pure	1.5	0.25	2.0	3.289	0.338	1.117	0.9725	97.7472	139.3984
	5	0.25	2.0	3.860	0.199	0.310	0.9819	3.2071	4.1966
	10	0.25	2.0	13.498	0.007	0.221	0.9345	4.7034	7.0811
	5	0.50	2.0	2.558	0.268	0.421	0.9384	9.6206	13.4835
	5	1.00	2.0	1.621	1.040	0.453	0.9677	27.9440	36.7528
	5	0.50	1.0	4.882	0.386	66.091	0.8242	15.6611	23.5167
	5	0.50	4.0	3.324	0.416	89.003	0.9834	7.4051	10.8617
CP-MPTES	1.5	0.25	1.9	1.617	0.833	0.752	0.9789	7.3459	10.1883
	5	0.25	1.9	3.306	0.558	0.663	0.9899	4.0571	6.8257
	10	0.25	1.9	5.095	0.279	0.430	0.9013	11.5642	16.5746
	5	0.50	1.9	1.765	0.237	0.754	0.9517	8.6375	15.7194
	5	1.00	1.9	1.458	0.014	0.837	0.8919	9.1825	14.8083
	5	0.50	1.0	3.863	0.279	0.540	0.9349	8.4096	13.4093
	5	0.50	3.5	2.047	0.843	0.735	0.9788	10.6977	16.2903
CP-RR	1.5	0.25	1.9	3.715	0.352	0.315	0.9894	5.2318	6.8993
	5	0.25	1.9	4.730	0.494	0.524	0.9488	9.3627	14.7277
	10	0.25	1.9	7.251	0.364	0.252	0.8197	21.0139	27.0412
	5	0.50	1.9	2.177	0.411	0.675	0.9852	2.8324	4.9787
	5	1.00	1.9	1.917	0.449	0.824	0.9106	5.8926	10.3243
	5	0.50	1.0	6.702	0.119	0.430	0.7807	12.2659	20.9858
	5	0.50	3.5	3.142	0.581	0.552	0.9913	4.2681	7.0929

Note: F (mL min^{-1}), C_o (mM), Z (cm), k_{TH} (mL $mmol^{-1}$ min^{-1}), Q_{TH} (mmol g^{-1})

Table S5. Bohart-Adam model parameters of Hg(II) and MeHg(II) adsorption onto CP adsorbents at different Z, F and C_o

Samples	F	C_o	Z	k_{BA}	N_o	r^2	ARE	MPSD
Hg(II) adsorption								
CP-Pure	1.5	0.25	2.0	3.771	1.043	0.6926	108.4266	173.9487
	5	0.25	2.0	6.357	1.305	0.7943	53.4583	68.7431
	10	0.25	2.0	6.710	1.462	0.7312	33.4708	38.0154
	5	0.50	2.0	3.403	2.239	0.5966	51.3823	71.6732
	5	1.00	2.0	0.650	4.008	0.8019	18.0239	33.1854
	5	0.50	1.0	4.167	2.4580	0.6407	51.1530	72.9266
	5	0.50	4.0	6.847	1.011	0.8860	84.6085	220.8562
CP-MPTES	1.5	0.25	1.8	4.660	0.703	0.6555	147.0531	325.1005
	5	0.25	1.8	8.375	0.903	0.7889	43.7606	55.3716
	10	0.25	1.8	6.902	0.971	0.7729	39.5047	51.1287
	5	0.50	1.8	3.053	1.802	0.8826	57.0482	67.9220
	5	1.00	1.8	1.560	2.780	0.9116	11.7043	16.2913
	5	0.50	1.0	12.217	0.635	0.5458	43.9878	74.7893
	5	0.50	3.6	5.013	0.952	0.8872	39.5841	50.1405
CP-RR	1.5	0.25	1.9	3.643	0.884	0.8245	60.4742	111.8676
	5	0.25	1.9	4.123	1.711	0.7721	45.2957	61.6895
	10	0.25	1.9	11.957	0.998	0.8856	50.3260	124.6520
	5	0.50	1.9	3.300	2.354	0.7652	53.8782	76.7551
	5	1.00	1.9	1.598	3.460	0.8469	24.7745	33.3834
	5	0.50	1.0	11.756	1.673	0.6596	80.2207	109.9622
	5	0.50	3.8	2.514	1.671	0.9288	12.3794	20.2616
MeHg(II) adsorption								
CP-Pure	1.5	0.25	2.0	12.125	0.119	0.8948	17.7969	26.3633
	5	0.25	2.0	9.577	0.269	0.9228	11.9166	19.6494
	10	0.25	2.0	19.354	0.170	0.9071	16.9410	34.6892
	5	0.50	2.0	4.545	0.340	0.8181	16.4787	26.5018
	5	1.00	2.0	2.443	0.466	0.8095	7.1192	12.2555
	5	0.50	1.0	9.406	0.346	0.6482	18.3122	26.4761
	5	0.50	4.0	7.005	0.242	0.7274	25.6584	34.0147
CP-MPTES	1.5	0.25	1.8	6.560	0.284	0.9050	21.6538	26.2360
	5	0.25	1.8	8.893	0.383	0.7989	20.5265	28.7608
	10	0.25	1.8	10.217	0.357	0.6490	22.4559	34.8735
	5	0.50	1.8	3.602	0.687	0.6921	18.4089	24.4817
	5	1.00	1.8	3.166	0.704	0.6251	23.9154	34.6877
	5	0.50	1.0	6.387	0.526	0.6126	18.3362	23.9039
	5	0.50	3.6	7.355	0.345	0.8174	26.4561	32.3176
CP-RR	1.5	0.25	1.9	13.014	0.126	0.8902	38.9938	48.9526
	5	0.25	1.9	14.756	0.257	0.7480	43.4965	53.3702
	10	0.25	1.9	13.396	0.228	0.5618	20.1038	30.5872
	5	0.50	1.9	4.986	0.519	0.8813	14.2835	24.4236
	5	1.00	1.9	4.099	0.595	0.7183	20.2627	29.9785
	5	0.50	1.0	16.439	0.295	0.6098	20.5990	26.8557
	5	0.50	3.8	9.740	0.238	0.8836	15.6883	21.9422

Note: F (mL min^{-1}), C_o (mM), Z (cm), k_{BA} (L mol^{-1} min^{-1}), N_o (mol L^{-1})

Table S6. Yoon-Nelson model parameters of Hg(II) and MeHg(II) adsorption onto CP adsorbents at different Z, F and C_o

Samples	F	C_o	Z	$k_{YN}\times10^3$	τ	$t_{0.5}$	r^2	ARE	MPSD
Hg(II) adsorption									
CP-Pure	1.5	0.25	2.0	1.588	2870	2650	0.8241	113.9646	232.6994
	5	0.25	2.0	3.416	823	790	0.9602	22.7067	33.6988
	10	0.25	2.0	4.380	320	220	0.9070	20.0240	25.2064
	5	0.50	2.0	3.774	620	370	0.8307	21.3276	33.1692
	5	1.00	2.0	3.005	135	270	0.8974	6.8389	10.3243
	5	0.50	1.0	3.169	479	363	0.8999	29.0938	55.5401
	5	0.50	4.0	2.838	1656	1645	0.9732	8.8445	20.4969
CP-MPTES	1.5	0.25	1.8	2.531	1380	1330	0.9249	76.4737	199.2181
	5	0.25	1.8	5.699	416	340	0.9864	14.3608	20.5094
	10	0.25	1.8	8.760	102	75	0.9671	6.8875	10.1456
	5	0.50	1.8	3.876	392	340	0.9881	24.8577	33.7068
	5	1.00	1.8	4.906	244	225	0.9449	7.1215	12.1678
	5	0.50	1.0	11.223	72	40	0.8126	36.7210	81.8411
	5	0.50	3.6	2.614	1122	1160	0.9742	12.6556	19.8661
CP-RR	1.5	0.25	1.9	1.654	2108	2095	0.9572	33.8156	71.2745
	5	0.25	1.9	2.577	863	745	0.9724	18.8302	31.5768
	10	0.25	1.9	7.739	243	215	0.9848	6.4239	8.0112
	5	0.50	1.9	3.436	695	527	0.9473	26.3297	47.4321
	5	1.00	1.9	4.066	396	285	0.9802	11.0458	17.7190
	5	0.50	1.0	6.775	474	270	0.8523	67.0149	102.3657
	5	0.50	3.8	1.345	2068	2430	0.9724	6.5594	11.1773
MeHg(II) adsorption									
CP-Pure	1.5	0.25	2.0	7.881	193	250	0.9725	12.5335	17.7549
	5	0.25	2.0	9.381	34	35	0.9819	3.2071	4.1968
	10	0.25	2.0	29.597	2	-	0.9509	4.5072	7.1723
	5	0.50	2.0	15.179	9	-	0.9384	4.5853	6.6546
	5	1.00	2.0	16.737	40	-	0.9559	25.6788	34.4599
	5	0.50	1.0	12.128	34	10	0.8242	15.6611	23.5167
	5	0.50	4.0	8.291	135	120	0.9834	7.4049	10.8620
CP-MPTES	1.5	0.25	1.8	3.876	475	560	0.9789	7.3457	10.1885
	5	0.25	1.8	7.980	95	90	0.9899	4.0575	6.8265
	10	0.25	1.8	12.197	24	17	0.9013	11.5643	16.5747
	5	0.50	1.8	8.488	20	35	0.9517	8.6374	15.7193
	5	1.00	1.8	14.222	1	26	0.8919	9.1823	14.8083
	5	0.50	1.0	9.256	24	21	0.9349	8.4261	13.4305
	5	0.50	3.6	4.990	277	200	0.9788	10.6981	16.2912
CP-RR	1.5	0.25	1.9	8.901	202	190	0.9894	5.2315	6.8990
	5	0.25	1.9	11.206	84	75	0.9488	9.3780	14.7524
	10	0.25	1.9	17.176	31	6	0.8197	21.0139	27.0413
	5	0.50	1.9	10.185	35	36	0.9852	2.8323	4.9784
	5	1.00	1.9	18.072	19	33	0.9106	5.8925	10.3241
	5	0.50	1.0	16.035	10	36	0.7807	12.2658	20.9860
	5	0.50	3.8	7.402	201	220	0.9913	4.2691	7.0929

Note: F (mL min^{-1}), C_o (mM), Z (cm), k_{YN} (min^{-1}), τ (min) and t (min)